Organic Chemistry: An Indian Journal

Organic Chemistry
ISSN: 0974-7516

Research | Vol 15 Iss 3

Molecular Structure, Spectroscopic Properties, Molecular Docking Analysis and *in vitro* Anticancer Activity Studies on of Gabapentin Compounds

Uvarani R[1*], Menaka A[1], Ragavan I[2] and Anbarasan PM[2]

[1]Department of Physics, Thiruvalluvar Government Arts College, Rasipuram, Tamilnadu, India.

[2]Department of Physics, Periyar University, Salem, Tamilnadu, India.

[*]**Corresponding author:** Uvarani R, Department of Physics, Thiruvalluvar Government Arts College, Tamilnadu, India, E-Mail: anbuuvanithin@gmail.com

Received: November 09, 2020; **Accepted:** March 21, 2021; **Published:** March 28, 2021

Abstract

To investigate their electronic structures, Potential Energy Curves (PECs) of S_0 and S_1 states and vibrational spectral properties of gabapentin based derivatives namely GPN_1-GPN_4 are calculated by employing the Density Functional Theory (DFT) and Time-Dependent Density Functional Theory (TD-DFT) methods of DFT at 6-311G^{++}(d,p) basis set using Gaussian 09 software. The vibrational assignments, $_1$H and $_{13}$C NMR chemical shifts of the complexes computationally and compared with experimental data. The calculated geometric parameters (bond lengths, bond angles, torsion angles), the mapped Molecular Electrostatic Potential (MEP), local reactivity descriptors and the Potential Energy Curves (PECs) of S_0 and S_1 states are scanned by varying H_{18}-N_7-H_{19} distance, etc. The molecular docking results suggest that the GPN_2 compound might exhibit inhibitory activity against Ca^{2+}/CAM-CaV2.2 IQ domain inhibitor.

Keywords: DFT; MEP analysis; Spectral properties; PECs; Molecular docking analysis

Introduction

Gabapentin or Aminomethyl Cyclohexanacetic Acid is a novel Antiepileptic Drug (AED) at present approved for the treatment of partial seizures neuropathic pain (nerve pain) [1], hot flashes, and restless legs syndrome conditions, such as diabetic neuropathy, central neuropathic pain, and painful diabetic peripheral neuropathy, post herpetic neuralgia [2]. Whilst gabapentin is considered to be better tolerated with fewer side effects than other antiepileptic drugs, treatment of nerve pain with oral gabapentin is still often limited by adverse effects such as posttraumatic stress disorder [3], dizziness, alcohol withdrawal, somnolence, hot flashes associated with prostate cancer treatment [4], and postoperative pain after cancer surgery [5, 6]. The topical gabapentin formulations or localized drug delivery has been controlled the adverse effect for NP whilst drug [5]. Furthermore, a recent approach is supported by *in vivo* study that has shown topical gabapentin formulations to be efficacious in rodent and porcine models for static or dynamic mechanical post-herpetic neuralgia and vulvodynia [6]. However, there is no licensed product comprising gabapentin available as a generic mediation in the United States or, somewhere else. This topical product is available as a "biological special" although, with reported compounds used as a treatment for seizures and neuropathic pain [7]. The bioavailability of gabapentin is comparatively light and strong doses (i.e. higher doses have lower bioavailability than lower doses). The bioavailability of gabapentin is approximately 27%-60% following 200 mg (threshold), 200 mg-600 mg (lower dose), 600 mg-900 mg (common), and 900 mg-1200 mg (higher dose) is about 5 hours-8 hours. Gabapentin is making unsaturated fats including olive oil and vegetable oil considerably boost the total amount of absorption for the reason eating a high heavy food considerably increases gabapentin's bioavailability and that meals measured down and thus decreasing gabapentin transporter saturation by increase gabapentin absorption [8].

In the present investigation, we describe the molecular structure, potential energy curves analysis and quantum chemical calculations have been performed for 2-(1-aminomethyl-cyclohexyl)acetic acid (GPN_1), methyl 2-(1-aminomethyl-cyclohexyl) acetate (GPN_2), 2-(1-(aminomethyl-cyclohexyl) acetamide (GPN_3), 2-(1-(aminomethyl-cyclohexyl) acetyl

Citation: Menaka A, Uvarani R, Ragavan I, Anbarasan PM. Molecular structure, spectroscopic properties, Molecular docking analysis and in vitro anticancer activity studies on of Gabapentin compounds. Org Chem Ind J. 2021;15(3):006

chloride (GPN_4). The detailed experimental FT-IR and FT-Raman spectra have been recorded and the calculated fundamental vibrational wavenumbers of Potential Energy Distribution (PED) have not been done so far. Further, the ^{13}C and ^{1}H Nuclear Magnetic Resonance (NMR), (UV-VIS) spectra, Molecular Electrostatic Potential (MEP) surface map, and frontier molecular orbital analysis were simulated and visualized. The chemical reactivity, stability, hardness, and softness values were performed by utilizing the HOMO-LUMO energies of the title molecules. For interesting molecular docking analysis of gabapentin-based different anchoring groups moiety followed by studying the in vitro biological and anticancer activities.

Experimental details

Gabapentin and solvent materials were supplied from Alfa Aesar chemical companies with no further purification. The FT-Raman spectrum of the compound was also recorded using Bruker RFS 27 spectrometer with 1064 nm lines of Nd: YAG laser source as excitation wavelength was obtained in the region from 4000 to 50 cm^{-1}. The Fourier transform infrared spectra are collected using Thermo Nicolet NEXUS 870 FT-IR spectrometer in the range of 400 cm^{-1} to 4000 cm^{-1} making KBr pellets of title the compound. The ^{1}H and ^{13}C NMR spectra were measured on Bruker FT-400 MHz spectrometer at room temperature and with $CDCl_3$ as a solvent.

Computational method

We studied the structural, electronic properties and the spectroscopic properties of GPN_1-GPN_4 was all the calculations presented here have been performed at the Becke‟s three-parameter hybrid exchange functional combining with Lee-Yang-Parr gradient-corrected correlation functional DFT/B3LYP/6-311G^{++}(d,p) basis set using quantum chemical calculations implemented with the help of Gaussian 09 Wprogram [9] package. The Gauss-View 5.0 can graphically display a variety of Gaussian results such as ground state optimized structure, molecular orbitals, NMR shielding density, MEP surface map, and animation of the normal modes corresponding to vibrational frequencies. The harmonic vibrational wavenumbers and all vibrational assignments were performed by the potential energy distribution calculated by using the VEDA 4 program [10]. The TD-DFT calculations of the title compounds were carried out using the PCM model with the same basis set considered for ground state optimizations. Electrostatic potential surface maps of the molecules have also been presented to view most negative electrostatic potential, most positive electrostatic potential, and zero potential regions. $_{1}H$ and $_{13}C$ NMR isotropic chemical shifts were calculated *via* the GIAO approach by applying DFT/B3LYP method with of 6-311G^{++} (d,p) [11, 12] basis set using in DMSO as a solvent were analyzed. The important chemical properties such as chemical hardness, softness, electron affinity electrophilicity index, ionization potential, and electronegativity. Molecular docking analysis was performed using AUTODOCK 4.2 [13] and PyMOL molecular graphics system to predict the binding pose, distance from the best mode (Å) of the title complexes.

Result and Discussion

Molecular geometry

The ground state optimized structural parameters or certain coordinates such as bond distances, bond angles, and dihedral angles of 1-4 complexes calculated by using DFT/B3LYP/6-311G^{++}(d,p) level of theory and accordance with atom numbering scheme is represented in (**FIG. 2)**.

R = OH
R = OCH_3
R = NH_2
R = Cl

FIG. 1. **General scheme of the compounds.**

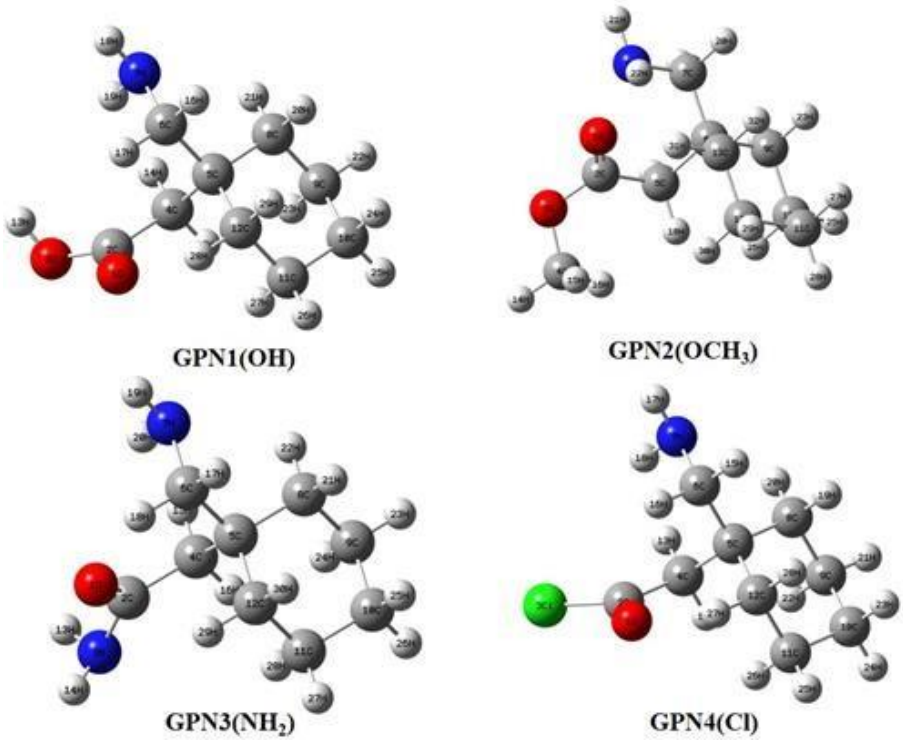

FIG. 2. **Showing the molecular theoretical structure of GPN_1-GPN_4 compounds.**

In this present work, geometry optimization parameters of molecules have been employed without symmetry constrain. The ground state optimized structure of GPN_1-GPN_4 belongs to the C_1 symmetry point group and has Global minimum energy of about E=558.0371,-597.2752,-538.2119, and -942.4537 Hartrees respectively. The calculated molecular parameter characterizes a good estimate and they are the bases of calculating other parameters including chemical structure, chemical kinetics, thermodynamic and spectroscopic properties. The optimized result of our calculations very high bond distances strong bond which is found to be C_2-O_1, C_4-C_2 bond distance of the ring varies in the narrow range 1.2359-1.5631 and smaller value of bond distances weak bond C_4-C_2, C_6-N_7 is 1.1079-1.1968Å. These bond angles mainly depend on the state of electronegativity (donate electrons) of the central atom. If the electronegativity of the central atom decreases, the bond angle also decreases. The bond distances, bond angles, and dihedral angles that show that the molecule is nearly perfectly planar are presented in **TABLE 1**.

TABLE 1. **Some selected optimized geometrical parameters (bond lengths (in Angstrom), bond angles (in degree), and dihedral angles (in degree)) of GPN_1-GPN_4 compounds.**

Optimized parameters	GPN_1(OH)	GPN_2(OCH_3)	GPN_3(NH_2)	GPN_4(Cl)
Bond distance (Å)				
C_2-O_1	1.2386	1.2359	1.4015	1.3432
C_2-O_3(1), C_2-O_1(2) N_3-H_{13}(3), C_2-Cl_3(4)	1.3858	1.2386	1.1968	1.2498
C_4-C_2	1.5612	1.5631	1.119	1.1079
C_6-N_7	1.4617	1.5525	1.1295	1.1923
Bond angle (°)				
C_6-N_7-H_{19}	112.191	112.6927	112.6865	112.6022
C_6-N_7-H_{18}	116.9586	116.9909	116.7863	116.9493
C_4-C_6-H_{18}	108.6775	108.5324	108.5416	108.5719
Dihedral angle (°)				
C_{11}-C_{12}-C_5-C_8	178.0352	179.3644	178.8163	178.4932
C_5-C_6-N_7-H_{18}	-87.4085	-71.0568	-85.7258	-88.5919

Vibrational spectral analysis

The fundamental vibrational wavenumbers of the most stable GPN_2 compound work to 32 atoms and 90 and belongs to the Cs symmetry point group for theoretical calculations. The comparative experimental and theoretical FT-IR and FT-Raman spectra of the title compound are shown in **FIG. 3** and **FIG. 4.**

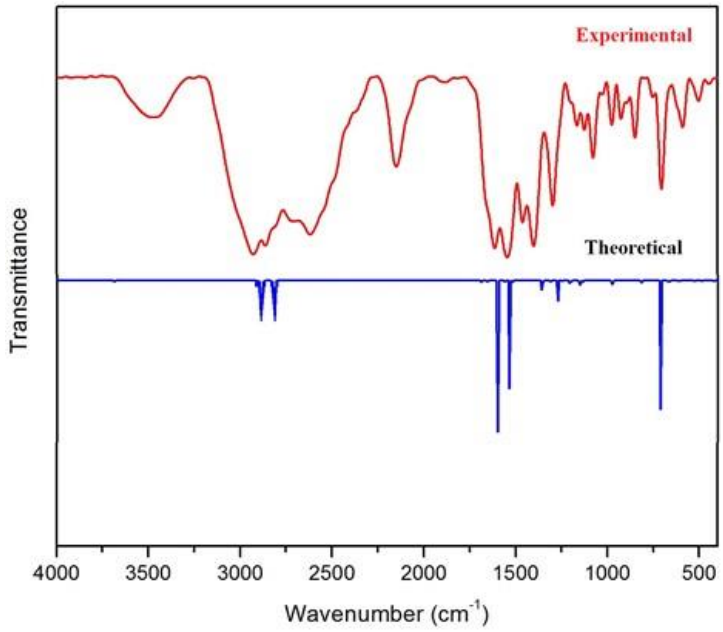

FIG. 3. **Experimental and calculated FT-IR spectra of GPN_2 compound.**

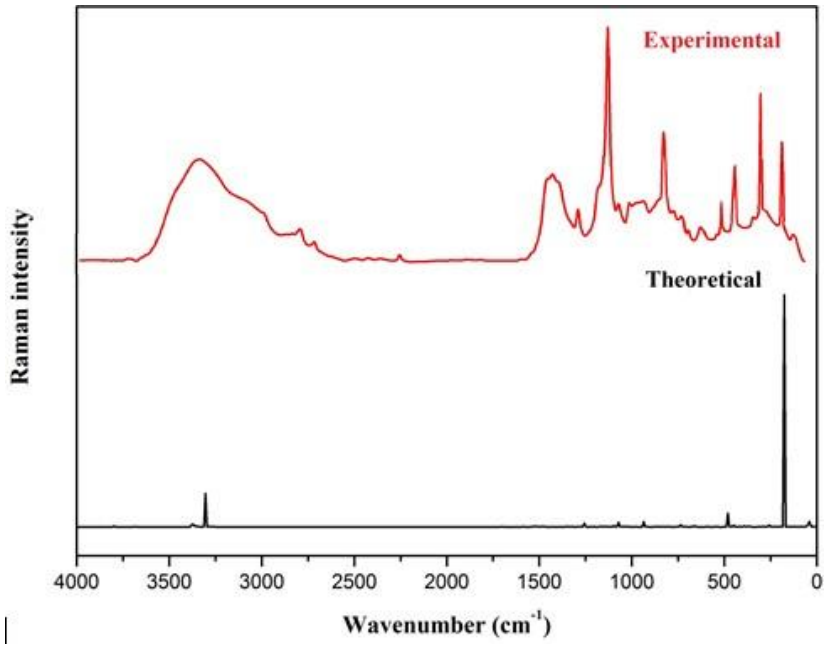

FIG. 4. **Experimental and calculated FT-Raman spectra of GPN_2 compound.**

The FT-IR and Raman vibrational pattern includes many stretching, bending, and torsional vibrations that create many signals. The calculated vibration wave numbers were usually higher than the observed vibrational modes. This is expected because the theoretical calculations of the isolated molecule considered in the gas phase while the experimental

measurements were carried out in the solid phase. On the other hand, the selected theoretical wavenumbers are harmonic while the experimental ones are anharmonic frequencies are listed in **TABLE 2.**

TABLE 2. **The experimental and computed vibrational frequencies of the GPN_2 compound.**

Experimental value		**Scaled Wavenumber (cm^{-1})**			**Vibrational Assignments (%PED)**
IR	**Raman**	**Freq. cm^{-1}**	**IR_{int}**	**Raman act.**	
3634	3612	3799	6.283	55.858	υ NH (100)
-	3590	3684	6.262	180.289	υ NH (98), υ NH (93)
-	-	3374	12.404	97.2367	υ CH (69)
-	-	3372	70.981	40.1104	υ CH (16)
-	-	3366	2.382	31.2997	υ CH (66), υ CH (23)
-	-	3365	60.597	50.8162	υ CH (25)
-	-	3358	5.370	46.9836	υ CH (17), υ CH (11), υ CH (19)
-	-	3351	55.950	15.5791	υ CH (17), υ CH (18), υ CH (13)
-	-	3250	38.184	33.742	υ CH (46), υ CH (47)
-	-	3247	31.880	138.2835	υ CH (23), υ CH (24)
-	-	3237	25.2	40.8711	υ CH (73), υ CH (21)
-	-	3202	10.832	306.0172	$υ_s$ CH (35), υ CH (30)
-	-	3292	79.669	114.5729	υ CH (19), $υ_{as}$ CH (55)
-	-	3190	22.122	50.2863	$υ_s$ CH (16), υ CH (19, υ CH (10)
3175	3170	3188	57.010	34.2517	υ CH (25), $υ_s$ CH (29)
-	3063	3083	25.513	49.7747	$υ_{as}$ CH (25), υ CH (32)
3051	-	3081	14.708	32.6566	$υ_{as}$ CH (12), υ CH (13), $υ_s$ CH (23)
2967	2958	3061	42.906	83.1765	υ CH (21), $υ_{as}$ CH (73)
2941	2933	3058	58.119	80.6824	$υ_{as}$CH (22), υ CH (33)
-	1667	1696	46.435	11.4167	$β_{ipd}$ HNH (69), τ HNCC (13), τ HNCC(12)
-	-	1578	83.677	4.8581	υ OC (65)
-	-	1526	11.527	19.1146	β HCH (47), τ HCOC (13)
1530	-	1521	16.072	12.7554	β HCH (23, υ CC (37)
-	-	1516	38.811	11.6397	$β_{ipd}$ HCH (13), β HCH (29)
1510	1518	1512	50.486	19.3971	β HCH (36), υ CC (22)
-	1500	1511	4.471	12.9769	β HCH (25)
-	-	1508	3.392	4.3508	υ CC (54), β HCH (13)
1489	-	1495	1.652	12.6221	δ CH_3 (18), β HCH (63)
-	-	1484	2.560	10.7246	υ CC (65)
1466	1470	1474	15.874	5.9672	δ CH_3 (16), β HCH (36), β HCH (21)
1460	-	1462	27.762	16.84	$β_{ipd}$ HCH (66)
-	-	1421	14.992	1.0999	τ HCCC (20)
-	-	1394	1.590	2.8334	β HNC (25), $β_{ipd}$ HCN (14)
-	-	1357	0.694	4.4442	β HCC (13), τ HCCC (25)
-	-	1353	3.128	2.0557	υ CC (10)
-	-	1349	2.912	2.3425	τ HCCC (14)
-	-	1332	0.790	0.6877	υ CC (11), τ HCCC (12)
-	-	1325	6.835	3.7909	τ HCCC (24)
-	-	1317	2.758	4.5854	β HCC (27), τ HCCC (26)
-	-	1283	20.547	7.5869	β HCC (11, τ HCCC (14)
-	-	1279	11.655	12.7592	β HCC (13, τ HCCC (11)
-	-	1256	19.733	12.3022	β HCN (10, τ HCCC (26)
-	-	1251	21.813	14.701	τ HCCO (12)
-	-	1220	10.413	2.2768	$β_{ipd}$ HCC (10, β HCC (10)
-	-	1198	33.816	6.5428	β HCC (16), τ HCCC (10)
-	-	1164	0.9941	6.3211	β HCH (11), τ HCOC (25), τ HCOC (12)
-	-	1143	13.595	7.2132	β HCH (14), β HCH (11), τ HCOC (20)
-	-	1137	11.358	2.2871	υ CC (43), τ HCCO (12)
-	-	1133	10.561	4.6808	υ NC (32), β HCC (11)

-	-	1112	34.920	1.5284	β HCC (12), β HCC (20)
-	-	1102	258.85	2.7585	υ OC (12), υ OC (44)
-	-	1089	17.757	5.9843	υ OC (25), υ NC (14), υ CC (13)
-	-	1086	6.7086	4.3465	υ NC (11), υ CC (15)
-	-	1067	110.29	2.5426	υ OC (12), υ CC (15), β OCO (12)
-	-	1061	0.7395	9.8854	τ HCCC (16)
-	-	1032	20.531	6.4812	υ CC (14), τ HCCC (10)
-	-	1012	13.871	8.4821	τ HCCC (12)
-	-	974	1.3666	2.9389	υ CC (31)
-	-	930	3.6254	1.0128	υ CC (17)
-	-	917	2.0595	6.3576	υ CC (19)
-	-	904	2.3042	1.1497	β CCC (12)
-	-	874	8.3875	2.0044	τ HCCO (12)
-	-	844	0.4406	6.424	υ CC (26, υ CC (14)
-	-	805	36.206	10.1452	υ OC (15), υ CC (29)
-	-	796	15.363	0.9426	τ HCCC (14)
-	-	747	0.8877	4.1603	υ CC (11), τ HCCC (10), τ HCCC (10)
-	-	733	5.974	6.5851	υ CC (30)
-	-	710	122.45	3.156	β HNH (10), τ HNCC (17), τ HNCC (28)
-	-	659	14.833	8.7775	υ OC (17), β OCO (35)
-	-	584	16.461	2.6188	β OCO (11), β COC (12), τ OCCC (11)
-	-	537	14.033	1.554	β NCC (28), r CCCC (11)
-	-	490	2.1675	1.1167	OUT OCOC (10), OUT CCCC (13)
-	-	474	2.0907	0.7138	R CCCC (10)
-	-	443	4.9047	1.6941	β CCC (22), r CCCC (15)

C-H vibration modes

The C-H stretching is considered characteristic wavenumbers. In such differences are usually observed for C-H vibrations. The aromatic ring shows the occurrence of C-H stretching vibration modes in the range 3100 cm^{-1}-3000 cm^{-1} region [14,15], which is the normal bands in the region for ready identification of C-H symmetric and asymmetric stretching vibrations. The title compounds observed C-H stretching vibration modes are assigned 3175, 3051, 2967, 2941cm^{-1} in FT-IR and 3170, 3063, 2958, 2933 cm^{-1} in FT-Raman spectra, and the calculated scaled DFT/6311^{++}G (d,p) values are 3188, 3083, 3081, 3061, 3058 cm^{-1} have been bands assigned to C-H stretching vibrations respectively.

Aromatic ring vibration

Benzene or aromatic ring is commonly used in organic chemistry. Although we write benzene is a special six-carbon ring (hexagon) that includes three double bonds, each of the carbon represents the delocalized electrons of the molecule. The fundamental vibrational oscillations of an aromatic ring are not isolated but involve the entire molecule. Fortunately, the force constants do vary with the molecular structure in a fairly expected approach and therefore it is possible to different types of C-C bonds. Generally, the aromatic ring C=C and C-C stretching vibrations, known as semicircle stretching modes are normally found between 1625 cm^{-1}-1400 cm^{-1}. The aromatic structure shows the presence of C-C stretching vibrations assigned at 1530 cm^{-1}, 1510 cm^{-1}, and 3092 cm^{-1} in FT-IR spectra and 1518 cm^{-1} in FT-Raman spectra, and the corresponding values are 1521 cm^{-1}, 1512 cm^{-1}, 1508 cm^{-1}, 1484 cm^{-1}.

CH_3 vibration modes

The CH_3 stretching vibrations modes for the assignments of CH_3 group frequencies, fundamentally nine normal vibration modes can be associated to each Methyl group [16] namely, CH_3 ss-symmetric stretch; CH_3 ips-in-plane stretch; CH_3 ops-out-of-plane stretch; CH_3 ipb-in-plane bending ; CH_3 opb-out-of-plane bending vibrations; CH_3 in-plane rocking, CH_3 opr-out-of-plane rocking; CH_3 ipb-in-plane bending; tCH_3-twisting modes; CH_3 sb-symmetric bending and the aromatic ring out-of-plane bending modes of methyl group vibrations would be expected to be depolarized. In CH_3 groups are normally referred to as electron-donating substituents in the molecular system. The in-plane stretch is usually at higher frequencies than the symmetric stretch. The methyl C-H vibrations appear at lower frequencies than aromatic C-H stretching vibrations. The calculated wavenumber of in-of-plane bending and out-of-plane bending modes of CH_3 values are 1495, 1474, 1462 cm^{-1}. The observed CH_3 opb and ipb were assigned 1489, 1466, 1460 cm^{-1} in FT-IR and 1470 cm^{-1} FT-Raman spectra. The CH_3 group vibrations computed DFT/6311^{++} G (d,p) methods also show good agreement with the experimental data. The twisting

vibration frequencies are assigned within the characteristic range and reported. The methyl group out-of-plane bending vibrations are also assigned and identified.

NH vibration modes

The NH group gives rise to five or six fundamental vibration modes including asymmetric stretching (vas), symmetric stretching (*vs*), the in-plane deformations (scissoring, δsis and rocking, δroc) and the out-of-plane deformation (wagging, γwag and twisting, γtwi). The molecule under study possesses one N-H out-of-plane bending, one symmetric N-H stretching, and hence expected one N-H asymmetric stretching vibrations. The N-H group stretching wavenumbers are usually observed in the region 3500-3300 cm^{-1} [17]. The asymmetric and symmetric stretching modes of the NH group are observed at 3634 cm^{-1} in the FT-IR and N-H stretching vibrations were identified in FT-Raman at 3612, 3590 cm^{-1} respectively. The theoretical values for these stretching vibrations of GPN_2 were calculated at 3799, 3684 cm^{-1} with an average PED contribution of 100%. However, good agreement between calculated and experimental spectra is observed for frequencies.

Frontier molecular orbitals analysis

The HOMO and LUMO levels are very common quantum chemical parameters that play a role in determining the way the molecule interacts with another molecule. The difference between HOMO-LUMO energy gaps is important parameters such as chemical stability, reactivity, and electronic charge transfer properties of the molecules. It determines the energy required for the charge transition from the main stable in the ground state to an excited state in a molecule. **FIG. 5,** shows the behaviors of the HOMO and LUMO molecular orbital diagram and respective calculated energy values of the frontier orbital energies of the studied compounds are summarized in **TABLE 3**.

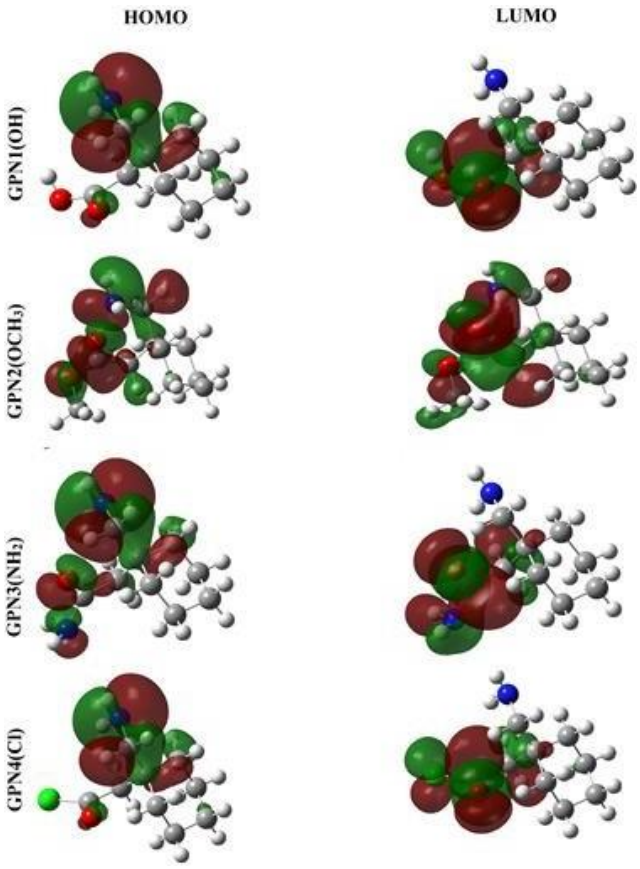

FIG. 5. **Graphics representation of frontier molecular orbitals**.

It was shown that for electron-withdrawing different functional substituted gabapentin GPN_1, GPN_2, GPN_3, and GPN_4 the HOMO level electron cloud is predominantly localized on the ring which has a lone pair of the benzene ring and OH, OCH_3, NH_2, Cl atoms bonded to ring with the highest density on carbons atoms. In HOMO orbital characterized by π-bonding over the whole molecule except C-C, C-C, C-C, C-N, C-O, C-H, H-O, and LUMO revealed anti-bonding orbital with no electron projection at these regions from C-C, C-C, C-C, C-N, C-O, C-H, H-O. As a result, it is expected that the energy difference between the HOMO and LUMO (HOMO-LUMO energy gap) displays the chemical activity of the molecule and the

calculated energy gap of the title compounds is 4.26 and 4.81 eV at the DFT/B3LYP levels, respectively. Likewise, these frontier molecular orbital formations of electron density localizations on HOMOs and LUMOs are supported by the nature of the transition is $\pi \rightarrow \pi^*$. This suggests the importance of considering these orbitals, especially GPN_2 and their corresponding eigen values upon studying their charge transfer properties. Also, the HOMO and LUMO energy values are used to compute global chemicals reactivity descriptors such as ionization potential (I), the electron affinity (A), Global electrophilicity (ω), the absolute electronegativity (χ), the chemical hardness (η) and softness (S) have been calculated at the same level theoretically by using HOMO and LUMO (ΔE) energy difference and are presented in **TABLE 3**.

TABLE 3. **Molecular Properties end energy gap (eV) between molecular orbitals involved in electronic transitions of GPN_1-GPN_4 compounds.**

Chemical reactivity	$GPN_1(OH)$	$GPN_2(OCH_3)$	$GPN_3(NH_2)$	$GPN_4(Cl)$
Ionization Potential (I)	-6.19	-4.45	-5.59	-6.09
Electron Affinity (A)	-1.38	-0.19	-1.06	-1.79
Energy gap (ΔE)	4.81	4.26	4.53	4.3
Electronegativity (χ)	3.785	2.32	3.325	3.94
Chemical Hardness (η)	2.405	2.13	2.265	2.15
Softness (S)	0.41580	0.46948	0.44150	0.46511
Global electrophilicity (ω)	1.2025	1.065	1.1325	1.075

NLO analysis

The calculated NLO properties such as molecular dipole moment, linear polarizability, and first-order hyperpolarizability of a molecular system, the quantum chemical calculations were performed by using DFT/B_3LYP method with 6-311G^{++} (d,p) level using Gaussian 09W program package. The molecules with large values of electronic dipole moment, polarizability, and hyperpolarizability are a measure of non-linear optical properties of the molecular system, which is linked with the electron cloud movement through π conjugated build of an electron. The theoretically calculated total molecular dipole moments (μ) of 1.2072 for GPN_1, 4.7808 for GPN_2, 2.8620 for GPN_3, 1.6353 for GPN_4 Debye, polarizability is equal to 1.073x10-23, 1.190x10-23, 1.086x10-23, 1.232x10-23 esu and first hyperpolarizability (β) of title compounds is 4.707x10-31, 5.758x10-31, 7.246x10-31, 2.695x10-31 esu, respectively as shown in **TABLE 4,** and thus results show that the title compounds is the best material for efficient nonlinear optical application.

TABLE 4. **Polarizability α_{tot} (x10-24esu) and Hyperpolarizability β (x10-31esu) of GPN_1-GPN_4 compounds calculated at the DFT/6-311^{++}G (d, p) level.**

Mol.	α	Δα	β_{tot}	μ
$GPN_1(OH)$	$1.073x10^{-23}$	$1.605x10^{-24}$	$4.707x10^{-31}$	1.2072
$GPN_2(OCH_3)$	$1.190x10^{-23}$	$1.051x10^{-24}$	$5.758x10^{-31}$	4.7808
$GPN_3(NH_2)$	$1.086x10^{-23}$	$1.320x10^{-24}$	$7.246x10^{-31}$	2.8620
$GPN_4(Cl)$	$1.232x10^{-23}$	$2.229x10^{-24}$	$2.695x10^{-31}$	1.6353

Molecular electrostatic potential analysis

The Molecular electrostatic potential maps are a helpful tool in understanding the physicochemical property relationship of a molecule since it shows the molecular properties including molecular shape, size, and color grading [18]. It is a calculation technique frequently used to analyzing the possible hydrogen binding site of the molecule by calculating the charge transfer interaction of a molecule. The most electronegative regions of MEP are related to electrophilic reactivity and the positive ones to nucleophilic reactivity for electron-donating and electron-accepting reaction at this visual presentation by using Gauss view 5.0 software MEP surface and molecular contour map is drawn for the title molecules as shown in **FIG. 6 and FIG. 7**.

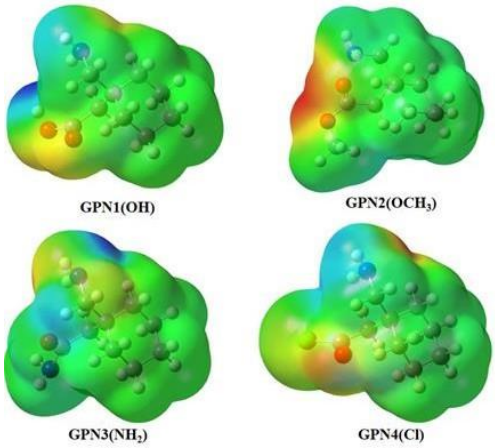

FIG. 6. **Molecular contour map of the electrostatic potential of the total density of GPN_1- GPN_4 compounds.**

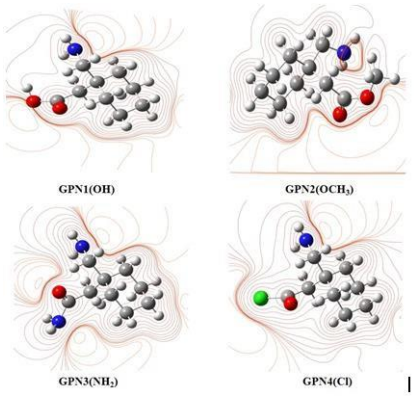

FIG. 7. **Molecular electrostatic counter map of GPN_1-GPN_4 compounds.**

The fitted electrostatic point charges alongside the electric potential V(r) calculated at DFT/B3LYP/6-311G^{++} (d, p) are given in **TABLE 5**.

TABLE 5. **ESP charges (e) and Electrostatic Potential V(r) values of GPN_1- GPN_4 compounds.**

Atom No.	**ESP charges (e)**				**Electrostatic Potential V(r) in a.u**			
	Electronegative atoms							
	GPN_1	**GPN_2**	**GPN_3**	**GPN_4**	**GPN_1**	**GPN_2**	**GPN_3**	**GPN_4**
8N	-0.717630	-0.72022	-0.67236	-0.62631	-17.764474	-17.3921	-0.2162	-17.5144
1O	-0.374437	-0.13540	-0.91947	0.086231	-17.486958	-17.1234	-0.2662	-17.3624
12C	-0.125330	-0.88085	-0.65284	-0.53242	-20.510692	-20.1151	-0.2342	-20.4219
4C	-0.009993	-0.46525	-0.13107	-0.13652	-20.585353	-20.3312	-0.2595	-20.1558
5C	-0.487875	-0.13992	-0.09068	-0.08489	-15.564211	-15.0249	-15.2558	-15.1070
2C	-0.052050	-0.08687	-0.21463	-0.27279	-15.252842	-15.1395	-15.1782	-15.5147
Electropositive atoms								
3O	0.592333	-0.52656	0.70041	0.309437	-15.268709	0.615845	0.229363	-0.56064
6C	0.210916	0.819031	0.74032	0.388483	-15.271719	-0.47179	-0.14533	0.40071
11C	-0.194115	-0.52484	-0.26353	-0.483054	-15.495509	-0.10583	-0.07314	-0.57917
10C	-0.428388	0.254198	-0.13736	-0.428776	-15.428388	0.100805	0.35791	-0.17283
13C	-0.004594	-0.10933	-0.21228	-0.063631	-15.749269	0.309074	0.346124	-0.06935
9C	0.056100	0.763356	0.229394	0.494789	-15.667291	0.147705	0.351429	-1.07864

As seen from Fig, the Intermediate potentials are assigned colors according to the following color regions: blue >green>red >yellow>orange. Different colors on the MEP surface map show electrostatic potential values of title compounds. The potential increases from red to blue. The regions with a negative electrostatic potential were found around the O atom of acetic acid whereas the regions with a positive potential were found around the H atoms.

Nuclear magnetic resonance analysis

In this study predicted chemical shifts of pharmaceuticals, the Gauge-Independent Atomic Orbital (GIAO) method [19] methods with optimized geometry using basis sets 6-311G^{++}(d,p) with B3LYP methods, have been interested in scientists, the compute the 1H and 13C chemical shifts are calculated and compared with experimental. In **TABLE 6,** the predicted $_{1}$H and $_{13}$C NMR chemical shifts are summarized by using the DFT/B3LYP\6-31G (d) methods in DMSO as a solvent.

TABLE 6. **Experimental and calculated $_{13}$C chemical shift [δ (ppm)] of GPN_1- GPN_4 compounds.**

Atoms	DFT	Experimental
GPN_1(OH)		
C	41.0	41.272400
C	88.2	85.018753
C	171.0	181.91114
GPN_2(OCH_3)		
C	26.9	23.371016
C	51.9	77.584347
C	38.6	-
C	173.1	196.446335
GPN_3(NH_2)		
C	27.2	29.339891
C	59.2	61.987373
C	179.3	213.63602
GPN_4(Cl)		
C	26.9	33.783877
C	36.6	36.224342
C	68.3	77.636029
C	178.7	220.86320

The Root-Mean-Square Deviations (RMSDs) between the experimental values with the corresponding computational values were performed by using DFT/B3LYP/6-311G^{++} (d,p) level theory. The experimental and theoretical NMR obtained from DFT has been shown in **FIG. 8.**

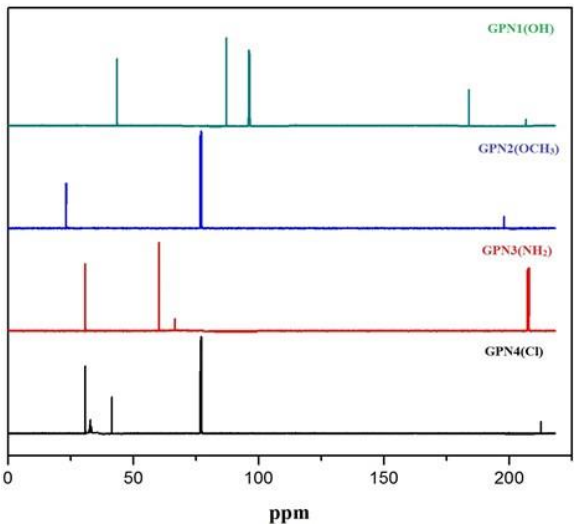

FIG. 8. **The $_{13}$C NMR chemical shifts spectra were recorded in the DMSO of the compounds.**

In our present investigation, chemical shift values of carbon atoms were determined in the range of 23.371016-220.8632 ppm, which agrees with literature values. The high chemical shift value of carbon atoms are compared to other aromatic carbons gives signals in overlapped areas of the spectrum with chemical shift values ranging from 25 ppm to 100 ppm. The oxygen atom in the methanol group results in the de-shielding of aromatic carbon atoms shows a downfield chemical shift of 181.911148 ppm (GPN_1), 196.446335 ppm (GPN_2), 213.636029 ppm (GPN_3), and 220.8632 ppm (GPN_4). Which are theoretically observed at 171.0 ppm, 173.1 ppm, 179.3 ppm, 178.7ppm, and show that the carbon atoms of methanol, methoxymethane, amino, and chloride groups in bioactivity. The scaled values are in good agreement with the experimental data. The $_1$H NMR chemical shifts show a singlet different function groups observed peaks upfield at 2.044854 ppm for OCH_3, 2.683420 ppm for OH group, 2.020196 ppm for OCH_3, and at 1.969190 ppm for Cl group and theoretically computed chemical shifts spectral assignments are listed in **TABLE 7**, The proton numbered H_{21}, H_{22} hydrogen atoms directly attached to the electronegative nitrogen shifts are shown in **FIG. 9**, respectively.

TABLE 7. **Experimental and calculated $_1$H chemical shift [δ (ppm)] of GPN_1- GPN_4 compounds.**

Atoms	DFT	Experimental
GPN_1(OH)		
H	2.15	2.149096
H	2.57	2.199787
H	2.0	2.044854
H	1.49	1.923143
H	1.46	1.640110
$GPN_2(OCH_3)$		
H	2.17	2.265715
H	2.57	2.382305
H	2.0	2.683420
H	7.49	7.603204
H	7.46	8.044854
$GPN_3(NH_2)$		
H	2.0	2.020196
H	2.10	2.130505
H	2.0	2.084416
H	1.49	-
GPN_4(Cl)		
H	2.76	3.942312
H	2.57	2.681987
H	2.0	1.969190
H	1.49	1.601293

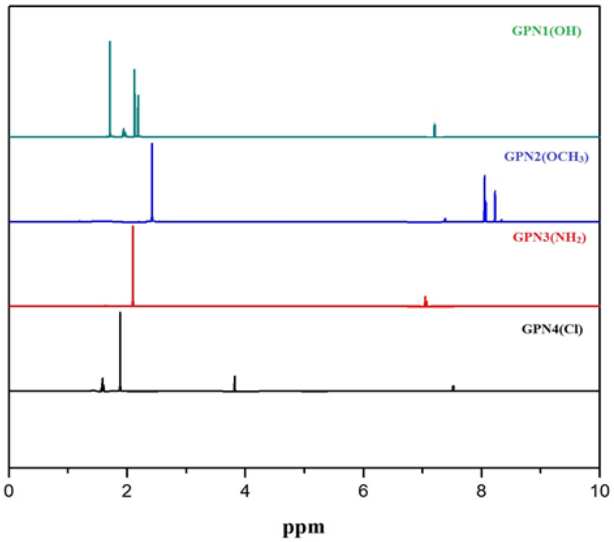

FIG. 9. **The $_1$H NMR chemical shifts spectra were recorded in the DMSO of the compounds.**

Mulliken charge analysis

Mulliken charges and natural atomic charges play an important role in the application of quantum chemical calculation such as electronic structure, dipole moment, molecular polarizability, and a lot of properties of molecular systems [20]. The electronic charge distribution over the atoms suggests the structure of electron-donor and electron-acceptor pairs involving the electronegativity equalization and charge transfer in the molecule. The Mulliken atomic charges and bar diagram representing the charge distribution is displayed in **FIG. 10** and **FIG. 11**.

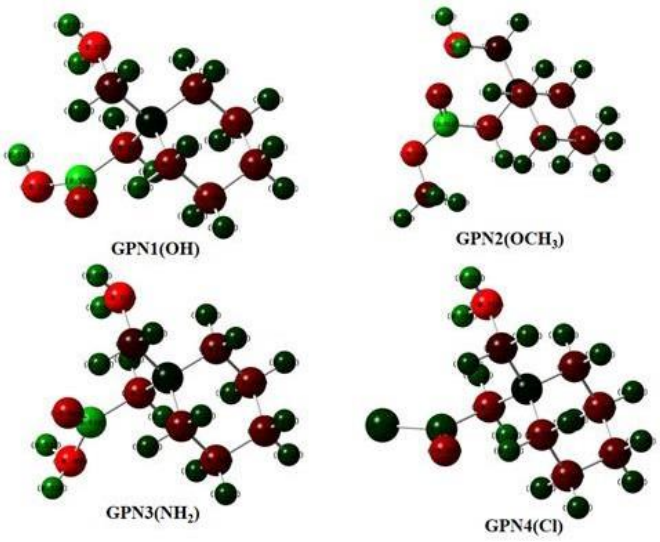

FIG. 10. **Optimized molecular charge distribution of GPN_1- GPN_4 compounds.**

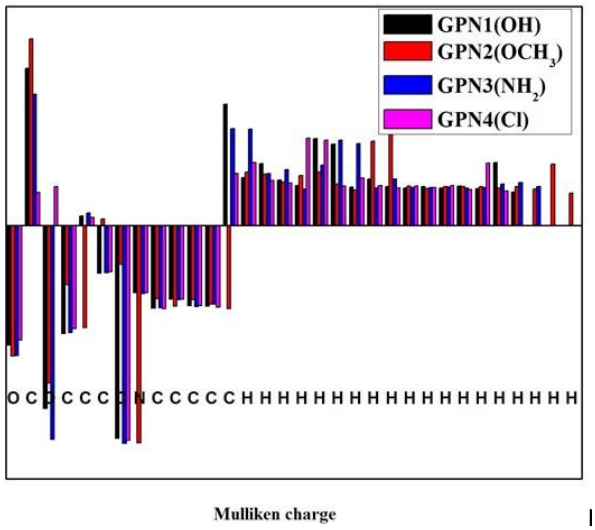

FIG. 11. **Mulliken charges distribution chart.**

The Mulliken atomic charges of the title molecule have been calculated by DFT/B3LYP method using 6-311G^{++} (d,p) levels of theory are collected in **TABLE 8,** from which it could be seen that the carbon atoms showed the highest positive charge is noted in C_{13}, C_2 and the lowest negative value is obtained in C_6, C_{10}, C_6, C_7, C_9 atoms. Among all the hydrogen atoms show net positive charge, respectively.

TABLE 8. **Values of the Milliken atomic charges (ZA).**

Mol.	GPN_1(OH)	GPN_2(OCH_3)	GPN_3(NH_2)	GPN_4(Cl)
1O	-0.3779	-0.41319	-0.4103	-0.36159
2C	0.49571	0.588105	0.413065	0.103209
3O	-0.57758	-0.49749	-0.67593	0.121715
4C	-0.34218	-0.18746	-0.33831	-0.32659

5C	0.028877	-0.32264	0.039167	0.025447
6C	-0.15128	-0.020707	-0.14996	-0.14586
7C	-0.67299	-0.12278	-0.68778	-0.67793
8N	-0.21277	-0.68726	-0.21573	-0.21302
9C	-0.26169	-0.23119	-0.25962	-0.26274
10C	-0.23276	-0.25566	-0.23437	-0.23284
11C	-0.25281	-0.23461	-0.25721	-0.25298
12C	-0.25495	-0.24979	-0.24953	-0.25776
13C	0.381537	0.26347	0.304922	0.163628
14H	0.15	0.16843	0.304042	0.197457
15H	0.194679	0.162334	0.162712	0.142132
16H	0.143041	0.136774	0.175855	0.132715
17H	0.1253	0.156848	0.113969	0.275528
18H	0.272882	0.168347	0.189785	0.268
19H	0.256175	0.130437	0.268819	0.123497
20H	0.120576	0.110854	0.258361	0.149256
21H	0.145954	0.265611	0.117254	0.124947
22H	0.122464	0.297938	0.146606	0.117122
23H	0.118258	0.124415	0.119228	0.124112
24H	0.122296	0.116267	0.120022	0.11867
25H	0.117099	0.121792	0.121579	0.125557
26H	0.123409	0.122435	0.117472	0.112695
27H	0.115533	0.122986	0.119528	0.196545
28H	0.198791	0.118025	0.129727	0.109061

Potential energy curves (PECs)

The conformational analysis [21, 22] of the gabapentin compounds is carried out through the potential energy surface scan (PES) in the present study by using DFT method 6-311G^{++} (d,p) level of theory. The conformational stability of GPN_1, GPN_2, GPN_3 and GPN_4 in the S_0 and S_1 states are calculated by potential surface scanning the amide group around the H_{18}-N_7-H_{19} bond is found to be 1.02 Å to 2.2 Å. The potential energy surface scan of the different conformers as a function of the angle of rotation is shown in **FIG. 12.**

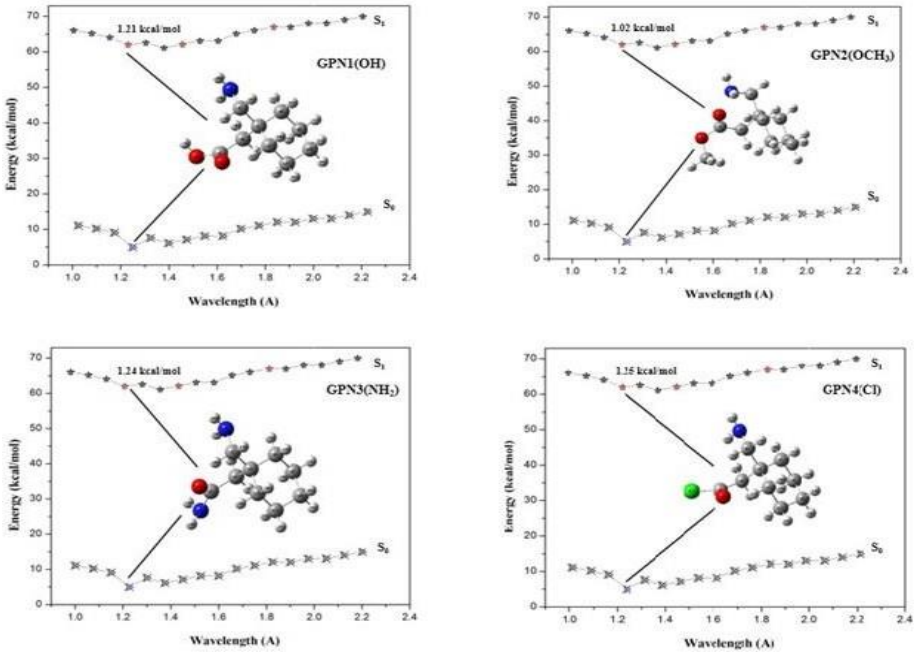

FIG. 12. **Profile of potential energy surface curves of GPN_1-GPN_4 compounds.**

It can be seen that there are no proton transfer reaction stationary points for the amide group form of Gabapentin derivatives in the S_0 state. The PES scan of the GPN_1-GPN_4 is 1.21, 1.24, 1.02, and 1.25 kcal/mol, which indicates that the potential barriers are small enough for proton transfer in the S1 state. Moreover, the S_1 state of reverse proton transfer barriers is 1.51, 1.52, 1.46, and 1.48 kcal/mol, respectively.

Molecular docking

It is generally believed that the small molecule drug contacts with active amino acid residues of the target enzyme to inhibit the activity of an enzyme. The PDB structures (www.rcsb.org) [3DVE] were downloaded and energy minimization of the protein structure [23]. Molecular docking analysis can help us to identify the binding types and the most important residues at the basis of the $Ca^{2+/}$CAM-CaV2.2 IQ activities, which paves new ways to design and synthesis a series of highly selective and potent $Ca^{2+/}$CAM-CaV2.2 IQ domain inhibitors. The four compounds with high, medium, and low activity can form hydrogen bonds with the protein. In Amino acids (GPN_1) Ile 85 forms a-alkyl interaction with a benzene ring and MET 145 (H-N-H), MET 76 (O=O-H) conventional hydrogen bonds with the amino radical and carboxylic acid group. Ile 85 forms alkyl interaction with a benzene ring and MET 145 (H-N), THR 146 (N-H) forms a-alkyl interaction with the amino radical group. In PHE 12 donor hydrogen bond with benzene ring interaction and TYR 1858 (N-H) forms pi-alkyl interaction with amine ring. In the compound, GPN4 forms H-bonds with Ile 85 a-alkyl interaction with a benzene ring, and MET 145 (N-H), MET 76 (O=N-H) form conventional hydrogen bonds with the amine group. These are the non-covalent interaction of the ligands GPN_1- GPN_4 with the substrate and are detailed in **FIG. 13** and **FIG. 14**.

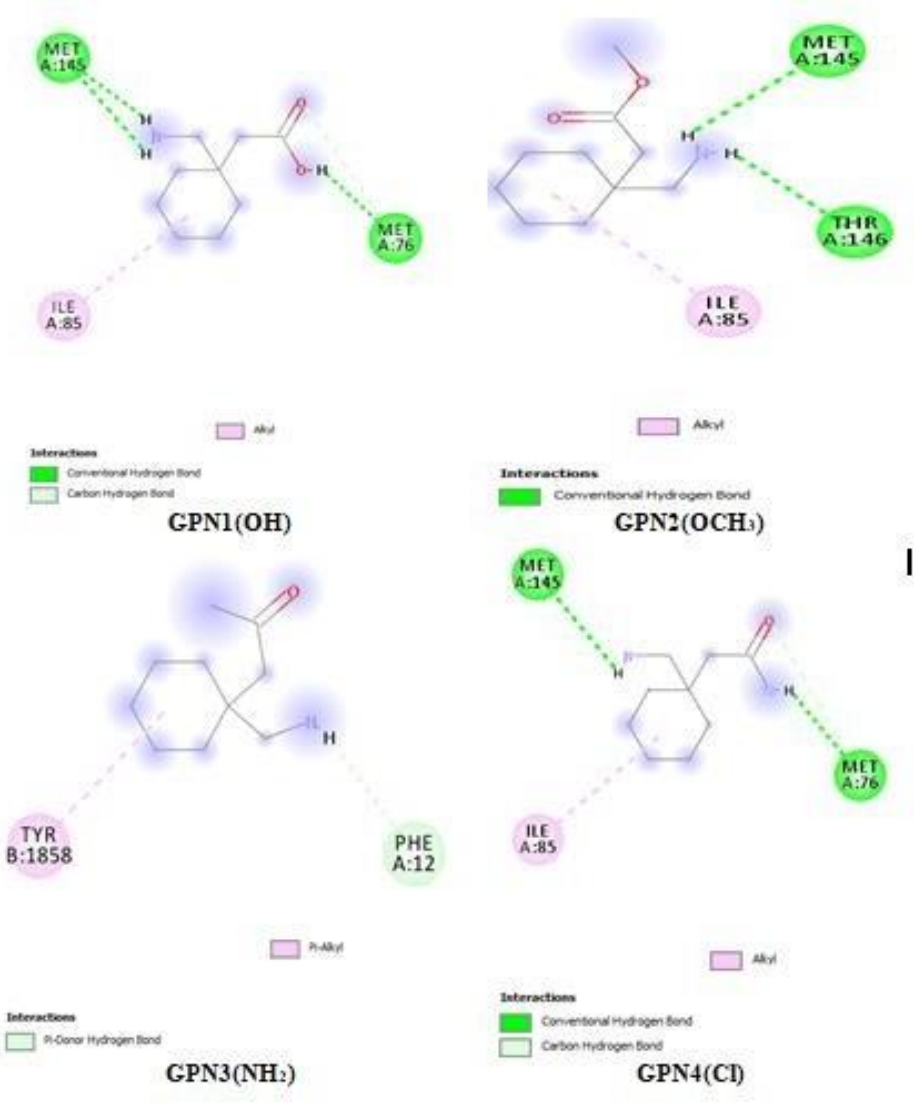

FIG. 13. **The Interaction of conventional hydrogen bonds amino acid residues of $Ca^{2+/}$CAM-CaV2.2 IQ domain inhibitors binding with the compounds.**

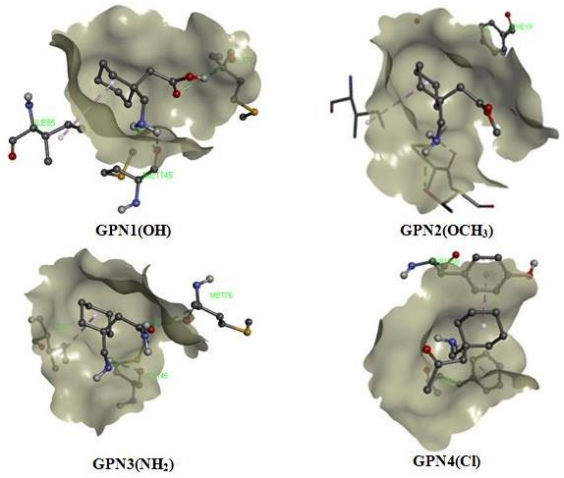

FIG. 14. **Predicted docking pose of GPN_1- GPN_4 compounds. Key residues of binding pocket are shown as sticks, Surface presentation of binding pocket and H-bonds are labeled.**

The docked ligands form stable complexes with Ca^{2+}/CAM-CaV2.2 IQ domain inhibitor which gives a good binding affinity value of -4.8kcal/mol for the GPN_2 compound. These binding affinity values of different poses of ligands with the same protein are tabulated in **TABLE 9**, These preliminary results suggest that the GPN_2 compound might exhibit inhibitory activity against Ca^{2+}/CAM-CaV2.2 IQ domain inhibitor.

TABLE 9. **The Docking, Bond distance, score, and H-bond interaction of best-fit ligands.**

Mode Affinity (kcal/mol)		**Distance from best mode (Å)**	
S. No	**Binding Affinity**	**RMSD/ub**	**RMSD/lb**
GPN_1(OH)			
1	-4.5	0	0
2	-4.3	16.711	14.944
3	-4.3	14.409	13.218
4	-4.2	13.511	12.512
5	-4.2	17.17	15.746
6	-4.1	4.12	2.789
7	-4.1	15.1	13.915
8	-4.1	26.064	24.984
9	-4.1	25.831	24.606
GPN_2(OCH_3)			
1	-4.8	0	0
2	-4.2	2.393	1.587
3	-4.3	25.612	24.174
4	-4.3	26.007	24.555
5	-4.3	17.207	16.38
6	-3.9	17.115	15.546
7	-3.9	25.603	24.332
8	-3.8	26.072	24.54
9	-3.7	26.202	25.042
GPN_3(NH_2)			
1	-4.5	0	0
2	-4.2	13.693	12.796
3	-4.2	4.175	2.742
4	-4.2	26.054	24.994
5	-4.2	13.702	12.475
6	-4.2	17.465	16.241
7	-4.1	13.503	12.396

8	-4.1	13.887	12.663
9	-4.3	13.222	12.079
GPN_4(Cl)			
1	-4.5	0	0
2	-4.5	14.516	13.562
3	-4.4	3.468	2.514
4	-4.2	3.428	2.726
5	-4.1	17.078	16.041
6	-4.1	14.361	13.514
7	-4.3	9.053	7.882
8	-4.3	24.049	23.077
9	-4	24.411	23.396

Conclusions

In the present study, the molecular geometry of the title molecules suggests that the different anchoring group"s moiety plays an important role in the intermolecular charge transfer interaction. The spectroscopic techniques such as FT-IR, FT-Raman for GPN_2 have been carried out by employing DFT/B3LYP method with 6-311G++ (d, p) level supported by PED contributions. The calculated normal modes of vibrations are in good agreement with the experimental results. The molecular electrostatic potential map shows that the regions with negative electrostatic potential sites are on electronegative O atoms and positive potential sites are around the hydrogen and carbon atoms. HOMO-LUMO energy gap and chemical stability descriptors of the title compounds were calculated. The result of the comparison between the experimental and calculated values of $_1$H and $_{13}$C NMR chemical shifts was calculated for title compounds. To further determine the scanning S_0 and S_1 states are calculated by potential surface scanning the amide group around the H_{18}-N_7-H_{19} bond. Molecular docking studies show that the GPN_2 compound might exhibit inhibitory activity against Ca^{2+}/CAM-CaV2.2 IQ domain inhibitor and strong affinity, distance from best mode (Å), suggesting that the compound may be candidates as anticancer drugs.

Acknowledgment

We are thankful to the sophisticated analytical instrumentation facility (SAIF) St. Joseph„s college, Thiruchirappalli, India for providing generous support in taking spectral measurements.

References

1. Jensen T.S. Anticonvulsants in neuropathic pain: rationale and clinical evidence. Eur J Pain. 2002;6:61-8.
2. Nicholson B. Gabapentin uses in neuropathic pain syndromes. Acta Neurol Scand. 2000;101:359-71.
3. Namour F, Olivier JL, Abdelmouttaleb I, Adjalla C, Debard R, Salvat C, Guéant JL. Transcobalamin codon 259 polymorphism in HT-29 and Caco-2 cells and Caucasians: relation to transcobalamin and homocysteine concentration in blood. Am J Hematol. 2001;97:1092-98.
4. Hansen M, Brynskov J, Christensen PA, Krintel JJ, Gimsing P. Cobalamin binding proteins (haptocorrin and transcobalamin) in human cerebrospinal fluid. Scand. J. Haematol. 1985;34:209-12.
5. Hansen M, Nexø E. Isoelectric focusing of apo-and holo-transcobalamin present in human blood. Identification of a protein complexing with transcobalamin. Biochimica et Biophysica Acta. 1989;18:209-14.
6. Begley JA, Colligan PD, Chu RC. Synthesis and secretion of transcobalamin II by cultured astrocytes derived from human brain tissue. J Neurol Sci. 1994;122:57-60.
7. Martin CJ, Alcock N, Hiom S, Birchall JC. Development and evaluation of topical gabapentin formulations. Pharmaceutics. 2017;9:31-48.
8. Fleet JL, Dixon SN, Kuwornu PJ, Dev VK, Montero-Odasso M, Burneo J, Garg AX. Gabapentin dose and the 30-day risk of altered mental status in older adults: A retrospective population-based study. PloS one. 2018;13:193134.
9. Lee C, Yang W, Parr RG. Development of the Colle-Salvetti correlation-energy formula into a functional of the electron density. Phys Rev. B 1988;37:785-9
10. Jamroz MH. Vibrational Energy Distribution Analysis (VEDA): scopes and limitations. Spectrochim Acta. A 2004; 114:220-30.
11. Becke AD. Density-functional thermochemistry. III. The role of exact exchange. J Chem Phys. 1993;98:5642-48.
12. Becke AD. Density functional exchange-energy approximation with correct asymptotic behavior. Phys Rev. A 1988; 38:3098-100.
13. Karelson M, Lobanov SV, Katritzky AR. Correlation of boiling points with molecular structure. 1. A training set of 298 diverse organics and a test set of 9 simple inorganics. J Phys Chem. 1996;100:10400.

14. Krishnakumar V, Prabavathi N. Scaled quantum chemical calculations and FTIR, FT-Raman spectral analysis of 2-Methylpyrazine. Spectrochim. Acta. A 2009;72:743-7.
15. Arıc K. Vibrational spectra of 4-hydroxy-3-cyano-7-chloro-quinoline by Density Functional Theory and ab initio Hartree-Fock calculations. Int J Chem Technol. 2017;1:24-9.
16. Kalsi PS. Spectroscopy of organic compounds. New Age International. 2007.
17. G. Socrates, Infrared, Raman Characteristic Group Frequencies Tables and Charts, Chichester, 3rd ed., Willey, 2001.
18. Govindasamy P, Gunasekaran S, Ramkumaar GR. "Natural bond orbital analysis, electronic structure and vibrational spectral analysis of N-(4-hydroxyl phenyl) acetamide: A density functional theory. Spectrochim Acta. A 2014;130:621-33.
19. Govindarajan M, Karabacak M. Spectroscopic properties, NLO, HOMO-LUMO and NBO analysis of 2, 5-Lutidine. Spectrochim Acta. A 2012;96:421-35.
20. Li H, Niu L, Xu X, Zhang S, Gao F. A comprehensive theoretical investigation of intramolecular proton transfer in the excited states for some newly-designed diphenylethylene derivatives bearing 2-(2-hydroxy-phenyl)-benzotriazole part. J Fluoresc. 2011;21:1721-28.
21. Liu YH, Mehata MS, Lan SC.TD-DFT study of the polarity controlled ion-pair separation in an excited-state proton transfer reaction. Spectrochim Acta. A 2014;128: 280-4.
22. Purkayastha P, Chattopadhyay N. Role of rotamerisation and excited-state intramolecular proton transfer in the photophysics of 2-(2′-hydroxyphenyl) benzoxazole, 2-(2′-hydroxyphenyl) benzimidazole and 2-(2′-hydroxyphenyl) benzothiazole: a theoretical study. Phys Chem Chem Phys. 2000;2:203-10.
23. Fleet JL, Dixon SN, Kuwornu PJ, Dev VK, Montero-Odasso M, Burneo J, Garg AX. Gabapentin dose and the 30-day risk of altered mental status in older adults: A retrospective population-based study. PloS one. 2018;13:193134.